



## NORMAL SHOCK WAVES IN WATER-VAPOUR FLOW

K.A. IBRAHIM\*, N.I. HEWEDY\*, N.H. MAHMOUD\*\* &amp; H. SHAFIEK\*\*\*

## ABSTRACT

In the present paper, the analysis of a normal shock wave with nonequilibrium upstream conditions in the water-vapour (wet steam) flow has been analysed theoretically and experimentally. The general flow equations in a water-vapour flow are formulated in the absence of the common assumptions of neglecting the rate of condensation and assuming equilibrium conditions prior to the shock. Also the flow properties through the relaxation zone have been obtained numerically. The results show that the behaviour of water-vapour flow through the relaxation zone behind the normal shock wave are mainly affected by the initial flow conditions; pressure, droplet size, wetness fraction and the amount of subcooling. Measurements for the pressure distribution of the water-vapour flow through a convergent-divergent nozzle are also carried out. In a quantitative comparison, the predicted pressure distribution could have a good agreement with the measured one.

## INTRODUCTION

Shock waves in water-vapour flows have received a considerable attention in various fields of basic fluid engineering. For examples;

- a) Accelerating and heating of liquid droplets by shock wave is useful for studying evaporation and ignition of liquid droplets.
- b) Wave motions produced by a explosions in the mixture and the flight of air-craft in rainy atmosphere.
- c) Acceleration of water drops by means of shock tubes for laboratory erosion experiments and for several purposes in space stations.

Shock waves consist, in general, of a leading discontinuity in the vapour phase velocity and temperature. Because of the finite time that is needed for the velocity and temperature of the droplets to adjust to those of the vapour phase, equilibrium between the two phases tends to be restored by the relatively

\* Associate Professor, \*\* Lecturer, \*\*\* Graduate student, Department of Mechanical Power Engineering, Menoufia University, Shebin El-Kom, Egypt.

slow processes of drag and heat transfer as the flow proceeds through the relaxation zone. Structure of shock waves in such media of gas droplet mixtures was investigated by Comfort, *et al* [1] and Lu and Chiu [2]. Very few studies have been developed to describe the influence of initial flow conditions on the flow properties through the relaxation zone behind a shock wave. For example, Cole, *et al*. [3] discussed the influence of the initial velocity and temperature lag on the flow behaviour through the relaxation zone behind a shock wave in a flow of gas-solid suspension. Also, the effect of water droplets on the flow properties through the relaxation zone developed behind strong normal shock waves was studied by Rakib and others [4] as well as by Amanbayev [5].

The aim of the present work is to study, theoretically and experimentally, the effect associated with changes in the initial conditions ( $P$ ,  $d$ ,  $Y$  and  $\Delta T$ ) on the behaviour of the flow parameters in the relaxation zone behind a shock wave. Furthermore, these conditions are shown to have radical influences on the relaxation zone characteristics.

#### GOVERNING EQUATIONS

Wet steam is considered herein as a homogeneous mixture from vapour and monodispersed incompressible spherical water droplets occupies negligible volume. We consider the vapour density is low enough so that it is considered thermally and calorically perfect. In order to show the shock wave effects on the behaviour of droplet growth, the investigated steam can be taken highly wet when nucleation disappeared (i.e., number of droplets remains constant). Water droplets are considered with size less than  $5 \mu\text{m}$ , such that the droplets velocity relative to the vapour one differs by 1-2%. Also, the pressure within the droplets is substantially equals to the pressure of the surrounding vapour. We shall additionally assume that the water droplets are with constant enthalpy equals to that of saturated water.

Based on the above assumptions and referring to Fig. 1, the governing equations of the wet steam flow can be expressed, as in [6], in the steady state and under the one dimensional approximation for the variable area passages as;

Continuity equations for the vapour and water phases:

$$\frac{d}{dx} (\rho_g . A . C.) + N . Q = 0 \quad \dots\dots (1)$$

$$u . \frac{dm}{dx} = Q \quad \dots\dots (2)$$

Equations of momentum for vapour and water phases:

$$A . \frac{dP}{dx} + N . DR . + \rho_g . A . C . \frac{dc}{dx} = 0 \quad \dots\dots (3)$$

$$DR = mu . \frac{du}{dx} - (c-u) . Q \quad \dots\dots (4)$$

Energy equation for the two-phases:

$$A \cdot \rho_g \cdot C^2 \cdot \frac{dc}{dx} + (N \cdot u) \cdot m \cdot u \cdot \frac{du}{dx} + A \cdot \rho_g \cdot C \cdot \frac{dh_g}{dx} + (N \cdot u) \cdot m \cdot \frac{dh_f}{dx} - N \cdot u \cdot (h_{fg} + \frac{c^2 - u^2}{2}) \cdot \frac{dm}{dx} = 0 \quad \dots\dots (5)$$

Equation of state in differential form is expressed by;

$$\frac{1}{p} \cdot \frac{dP}{dx} = \frac{1}{\rho_g} \cdot \frac{d\rho_g}{dx} + \frac{1}{T_g} \cdot \frac{dT_g}{dx} \quad \dots\dots (6)$$

Temperature variation of the droplets can be obtained from Clausius-Clapeyron's equation as

$$\frac{dT_s}{dx} = \frac{T_s \cdot v_{fg}}{h_{fg}} \cdot \frac{dP}{dx} \quad \dots\dots (7)$$

Watness fraction may written as

$$Y = 1 - X = n \cdot \frac{\pi}{6} \cdot d^3 \cdot \rho_f \quad \dots\dots (8)$$

Drag force between vapour and droplets for small slip between the two phases is expressed by

$$DR = \frac{3 \pi \mu_g d}{1 + 2.7 Kn} \quad \dots\dots (9)$$

where; Kn is given by

$$Kn = \frac{1.5 \mu_g}{d \cdot \rho_g} \left( \frac{1}{R_g \cdot T_g} \right)^{1/2}$$

The latent heat released to the droplets by the condensing vapour is therefore returned by conduction/convection to the vapour phase as in the following heat balance

$$h_{fg} \cdot \dot{Q} = \alpha \cdot (\pi d^2) \cdot (T_f - T_g) \quad \dots\dots (10)$$

where:  $\alpha = \frac{2 \lambda_g}{d} \cdot \left( \frac{1}{1 + 3.18 Kn} \right)$

Solving the above governing equations (Eqs. 1-5) with the aid of the supplementary equations (Eqs. 6-10) will give the following differential equations:

Droplet size variation:

$$\frac{dd}{dx} = \frac{4 \lambda_g \cdot (T_f - T_g)}{h_{fg} \cdot u \cdot \rho_f \cdot d \cdot (1 + 3.18 Kn)} \quad \dots\dots (11)$$

- Wetness fraction variation:

$$\frac{dY}{dx} = n \cdot \frac{\pi}{2} d^2 \cdot \rho_f \cdot \frac{dd}{dx} \quad \dots\dots (12)$$

- Droplets velocity variation:

$$\frac{du}{dx} = \frac{6DR}{\pi \rho_f \cdot u \cdot d^3} + \frac{3(c-u)}{d} \cdot \frac{dd}{dx} \dots\dots\dots (13)$$

- Vapour phase velocity variation:

$$\begin{aligned} \frac{dc}{dx} = & \left\{ \frac{1}{A} \cdot \frac{dA}{dx} + \frac{N \cdot U \cdot \pi \cdot \rho_f \cdot d^2}{2 \cdot A \cdot C \cdot \rho_g} \left[ 1 - \left( \frac{h_{fg}}{C_{pg} \cdot T_g} + \frac{c^2 - u^2}{2C_{pg} \cdot T_g} \right) \right] \cdot \frac{dd}{dx} \right. \\ & + \frac{N \cdot U^2 \cdot m}{T_g \cdot A \cdot \rho_g \cdot C \cdot C_{pg}} \cdot \frac{du}{dx} - \frac{N^2 \cdot U \cdot m \cdot C_f \cdot T_s \cdot V_{fg} \cdot DR}{T_g \cdot A^2 \cdot \rho_g \cdot C \cdot C_{pg} \cdot h_{fg}} - \frac{N \cdot DR}{P \cdot A} \left. \right\} / \left( \frac{\rho_g \cdot C}{P} - \frac{C}{T_g \cdot C_{pg}} \right) \\ & - \frac{1}{C} + \frac{N \cdot U \cdot m \cdot C_f \cdot T_s \cdot V_{fg}}{T_g \cdot A \cdot C_{pg} \cdot h_{fg}} \dots\dots\dots (14) \end{aligned}$$

- Flow pressure variation:

$$\frac{dP}{dx} = - \frac{N \cdot DR}{A} - \rho_g \cdot C \cdot \frac{dc}{dx} \dots\dots\dots (15)$$

- Vapour temperature variation:

$$\frac{dT_g}{dx} = \frac{T_g}{A} \cdot \frac{dA}{dx} + \frac{T_g}{C} \cdot \frac{dc}{dx} + \frac{T_g}{P} \cdot \frac{dP}{dx} + \frac{N \cdot U \cdot \pi \cdot \rho_f \cdot d^2 \cdot T_g}{2 \cdot A \cdot C \cdot \rho_g} \cdot \frac{dd}{dx} \dots\dots\dots (16)$$

- Vapour density variation:

$$\frac{d\rho_g}{dx} = - \left[ \frac{\rho_g}{C} \cdot \frac{dc}{dx} + \frac{\rho_g}{A} \cdot \frac{dA}{dx} + \frac{N \cdot U \cdot \pi \cdot \rho_f \cdot d^2}{2 \cdot A \cdot C} \cdot \frac{dd}{dx} \right] \dots\dots\dots (17)$$

- Liquid phase temperature variation is obtained using Eq. (7).

### NUMERICAL SOLUTION

The set of the differential equations, presented above, are solved numerically using the 4<sup>th</sup> order Runge-Kutta-Merson method with a stable finite interval  $\Delta x$ .

The vapour phase parameters behind the shock wave are calculated using Rankin-Hugoniot relations and the droplets are assumed to pass through the shock unaffected. The parameters behind the shock are then regarded as the inlet conditions for the relaxation zone program which are used to follow the further changes in the flow. Computation of the variations of the relevant vapour and droplets parameters has been carried out using PDP-11/70 Model main frame computer.

The calculations were made for the following initial flow conditions:

$$P_o = 2.2, 8.8 \text{ and } 16 \text{ bar}; \quad d_o = 0.5, 1 \text{ and } 3 \mu\text{m};$$

$$Y_o = 0.0005, 0.002 \text{ and } 0.005; \quad \Delta T_o = 1, 6 \text{ and } 10^\circ\text{K}.$$

#### THEORETICAL RESULTS AND DISCUSSION:

The results described here are for the nozzle profile shown in Fig. 2. Nozzle with this profile has been used in parallel experimental studies. During the calculations values of  $C_o = 10.42 \text{ m/s}$ ,  $u_o/c_o = 0.99$  and  $\Delta T_o = 10^\circ\text{K}$  were kept constant; while the other initial flow conditions at the nozzle inlet were changed.

Fig. 3 shows the effect of changing the initial pressure on the variation of pressure behind the shock wave which occurred in the divergent section. The results were obtained for  $d_o = 0.5 \mu\text{m}$  and  $Y_o = 0.5\%$ . In this figure, it is apparent that the pressure recovery throughout the relaxation zone behind the shock decreases with the pressure increasing at the nozzle inlet. Also when  $P_o$  is increased, the length of the relaxation zone following the shock decreases. This means that the flow reached to its equilibrium conditions early in the case of high value of  $P_o$ . Fig. 4, shows the behaviour of the vapour and droplet velocities through the relaxation zone for different values of  $P_o$ . Immediately following the shock, the droplet velocity ( $U$ ) is greater than the vapour velocity ( $C$ ). This will cause a negative value for the momentum exchange between the phases, and this together with the negative heat transfer term (see Fig. 5) result in a fast decline on the vapour velocity. This rate of decline of velocity decreases with approaching equilibrium, since the slip velocity becomes smaller. The temperature variations behind the shock wave for different values of  $P_o$  are shown in Fig. 5. From this figure, it will be seen that the further increase of the initial pressure leading to deviate the wet steam out of thermal equilibrium and to extend the relaxation zone. Figs. 6 & 7 show the variations of droplet size and wetness fraction behind the shock wave. These results indicate that the pressure variation at nozzle inlet will have a pronounced effect on the evaporation rate behind the shock wave. The rate of droplet evaporation and wetness dissipation are increasing with any further increase of the wet steam initial pressure. These results may be confirmed by Amanbayev [5].

Figs. 8-12 show the effect of initial droplet size on the flow properties through the relaxation zone. The calculations were made for  $P_o = 2.2 \text{ bar}$  and  $Y_o = 0.5\%$ . From these figures it can be seen that the length of the relaxation zone increases with an increase in initial droplet diameter. Also as the  $d_o$  increases the vapour and droplet velocities have higher values than those for small droplet diameters, see Fig. 9. As the droplet diameter is reduced the peak value of the gas temperature is also reduced, Fig. 10, indicating that the heat transfer gradually becomes a more important influence on the flow. From all the

figures, it is easy to see that the equilibrium conditions are approached more rapidly with a reduced droplet diameter. The reduced diameter increases the number of droplets present and the total surface area, thus increasing the heat transfer rate and the initial total droplet drag. Figs. 11 & 12 illustrate the effect of the initial droplet size on the evaporation rate behind the shock wave. From these figures, it can be concluded that the rate of evaporation and wetness dissipation is decreased with increasing the initial droplet size.

The effect of the initial wetness fraction variation on the flow parameters throughout the relaxation zone is shown in Figs. 13-17. The initial conditions were chosen to be  $P = 2.2$  bar,  $d_0 = 0.5 \mu\text{m}$  and  $\Delta T = 10^\circ\text{k}$ . In these figures, it can be seen that the length of the relaxation zone increases with a decrease in the value  $Y_0$ . This means that the equilibrium conditions are approached more rapidly with increased  $Y_0$ . Also the vapour and droplet velocities decrease with an increase in  $Y_0$ , while the pressure and saturation temperature are increased. These trends result from the droplet drag and heat transfer being increased because there are a large number of droplets present at the higher wetness fraction. From Figs. 16 & 17, it is apparent that the variation of the initial wetness fraction at nozzle inlet will have a distinct effect on the evaporation rate behind the shock wave. This effect is produced due to the increased temperature lag between the two-phases.

Figs. 18 - 22 show that the variation of the initial subcooling at the nozzle entrance does not have any pronounced effect on the flow pressure and the two-phase velocities within the relaxation zone. This effect may be explained with the small variations in the vapour density due to the changes in subcooling. In Figs. 18 - 22 the results were obtained for  $P = 2.2$  bar,  $d_0 = 0.5 \mu\text{m}$  and  $Y = 0.5\%$ . From Fig. 20, it will be seen that the increase of  $\Delta T_0$  causes the flow to deviate from the equilibrium and to increase the length of the relaxation zone. This feature is generated from the monotonic variation in the saturation temperature of the water-vapour mixture. Figs. 21 & 22 illustrate that as the initial subcooling increases the rates of droplets evaporation and wetness dissipation are decreased monotonically.

#### EXPERIMENTAL WORK AND COMPARISON WITH THEORY:

A schematic diagram for the experimental setup is shown in Fig. 23. It consists of a steam vessel (1) supplies wet steam from a fire-tube boiler of 1 ton/hr wet steam capacity at 6 bar. Exhaust steam from the steam vessel is condensed in a surface condenser (6) and is rated in a metring tank. The investigated nozzle (2) was made from brass and manufactured with the profile shown in Fig. 2. During the experiments; the static pressure distribution along the nozzle axis, steam flow rate, static vapour temperature, and the wetness fraction at the nozzle entrance were measured. The axial pressure variation along the nozzle axis was measured by means of a Stodola search probe (3)

of nominal diameter 3.31 mm and is equipped with a pressure transducer (4). The probe is traversed in increments of 2 mm by rotating a calibrated dial. The vapour velocity; at the nozzle inlet; was obtained by measuring the steam flow rate, vapour pressure and temperature inside the vessel. A mercury-in-glass thermometer (8) was used to obtain the static temperature of the wet steam flow in the vicinity of nozzle entrance. Also, a pressure gauge was used to indicate the vessel pressure. The steam vessel also carries a throttling calorimeter (5) with mercury-in glass thermometer (8) in order to measure the dryness fraction of the wet vapour.

Fig. (24) presents a comparison between the predicted pressure values and the measured ones for a wet steam flow under initial conditions of  $P_{o1} = 2.2$  bar,  $C_o = 10.42$  m/s,  $Y_o = 0.006$  and  $\Delta T \approx 4^\circ\text{k}$ . This figure shows satisfactory agreement between the experimental results and the theoretical predictions throughout the relaxation zone.

### CONCLUSIONS

The behaviour of wet steam flow, behind the shock wave, through the supersonic flow nozzle was studied both theoretically and experimentally. The variation of pressure, vapour velocity, vapour temperature, droplet temperature, droplet velocity, rate of evaporation and rate of condensation in the relaxation zone has been shown to depend significantly on the initial flow conditions at the nozzle entrance. The rate of droplet evaporation and wetness dissipation are increasing with an increase in the pressure inlet and decreased by increasing the initial droplet size. Also the length of the relaxation zone is mainly depend on the initial flow conditions. Finally, a comparison between the theoretical and experimental results gives a reasonable agreement.

### REFERENCES

1. Comfort, W.J., Alger, T.W., Giedt, W.H. and Crowe, C.T., "Calculation of two-phase dispersed droplet-in-vapour flows including normal shock waves", Trans ASME, J. Fluids Eng., Vol. 100, p. 355 (1978).
2. Lu, H.Y., and Chiu, H.H., "Dynamics of gases containing evaporable liquid droplets under a normal shock", AIAA. J., Vol. 4, No. 6, p. 1008 (1966).
3. Cole, B.N., Baum, M.R., and Mobbs, F.R., "The influence of initial velocity and temperature lag on the relaxation zone behind a shock wave in a gas-solid flow", IMechE, Heat and Fluid Flow, Vol. 5, No. 2, p. 110 (1975).
4. Rakib, Z., Igra, O., Ben-Dor, G., "The effect of water droplets on the relaxation zone developed behind strong normal shock waves", Trans. ASME, J. Fluids Eng., Vol. 106, p. 154 (1984).
5. Amanbayev, T.R., "Structure of shock waves in gas-droplet suspensions", Fluid Mech., Soviet Res., Vol. 14, No. 3, p. 106 (1985).
6. Moore, M.J., and Sieverding, C.H. (Editors), "Two-phase steam flow in turbines and separators", Hemisphere Publ. Comp., Washington & London (1976).

7. Mahmoud, N.H., "Two-phase flow (Wet steam) in nozzles", Ph.D. Thesis, Mech. Eng. Dept., Menoufia University, Shebin El-Kom , Egypt (1986).

## NOMENCLATURE

$\alpha$	Heat transfer coefficient.
$\Delta T$	Amount of subcooling.
$\lambda$	Thermal conductivity.
$\mu$	Dynamic viscosity
$\rho$	Density.
A	Flow cross-sectional area.
C	Ansolute velocity of vapour phase.
$C_f$	Mean heat capacity of water.
$C_{pg}$	Isobaric specific heat capacity of vapour.
d	Droplet diameter.
DR	Drag force on a droplet.
h	Specific enthalpy.
Kn	Knudsen number.
L	Nozzle length.
m	Mass of a droplet.
n	Number of droplets per unit mass of water-vapour mixture.
N	Number of droplets per unit length.
P	Vapour pressure.
Q	Rate of mass increase of a droplet by condensation.
R	Gas constant (= 461.51 J/Kg .°k).
$T^g$	Temperature.
U	Droplet velocity.
v	Specific volume.
x	Distance in flow direction.
X	Dryness fraction.
Y	Wetness fraction.

## SUBSCRIPTS

f	Water phase-Frozen.
g	Vapour phase.
fg	Phase transition.
s	Saturation.
m	Mixture.
o	Initial conditions.

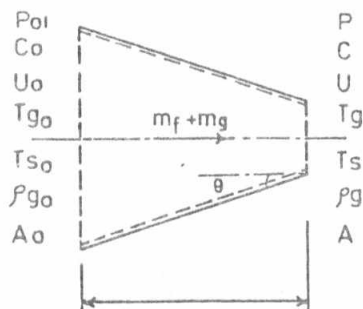


Fig. 1 : An elemental length of the flow .

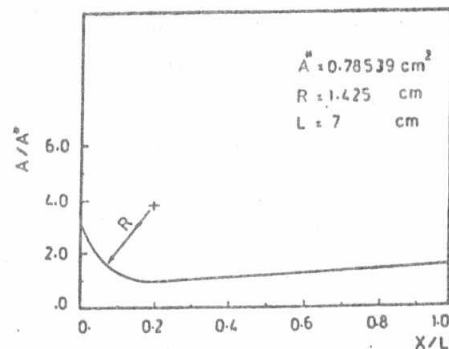


Fig. 2 : Nozzle profile .



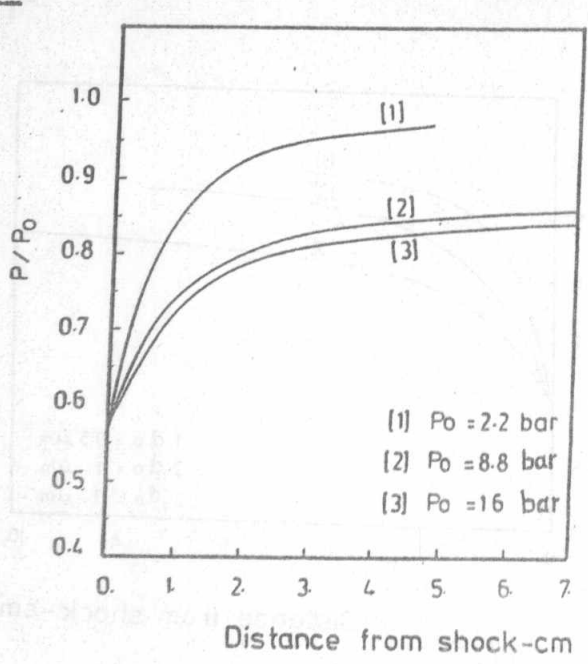


Fig. 3 : Variation of flow pressure along the relaxation zone (effect of  $P_0$ ).

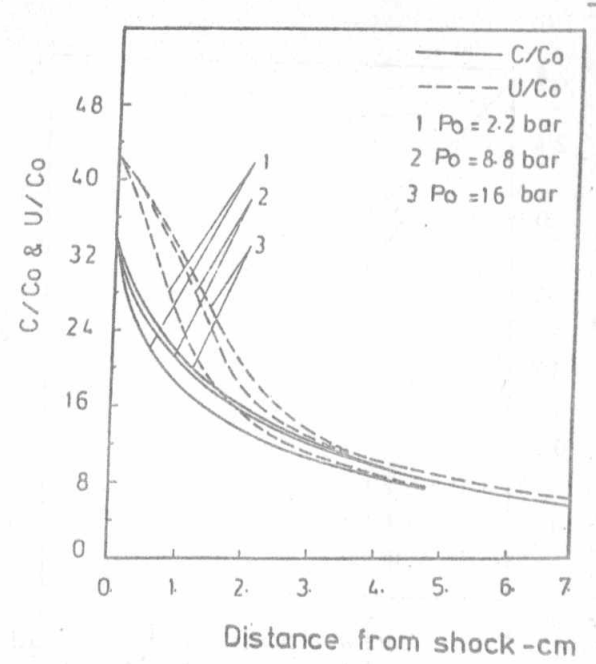


Fig. 4 : Variation of vapour and droplet velocities behind the shock wave (effect of  $P_0$ ).

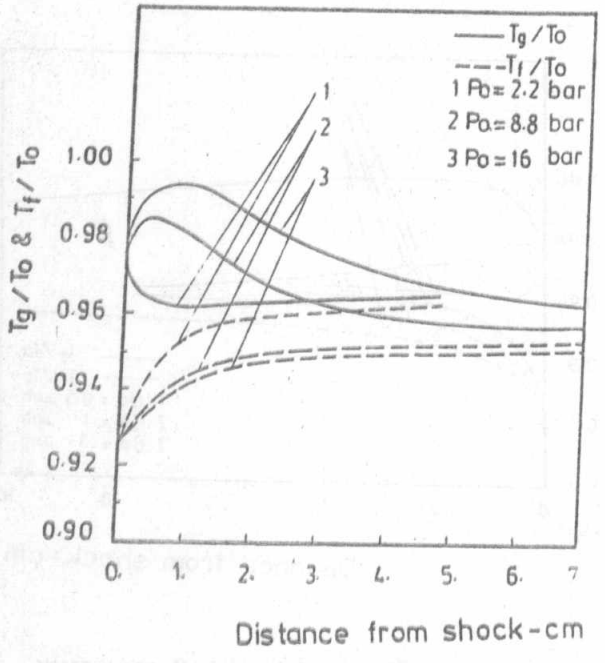


Fig. 5 : Variation of vapour and droplet temperatures behind the shock wave (effect of  $P_0$ ).

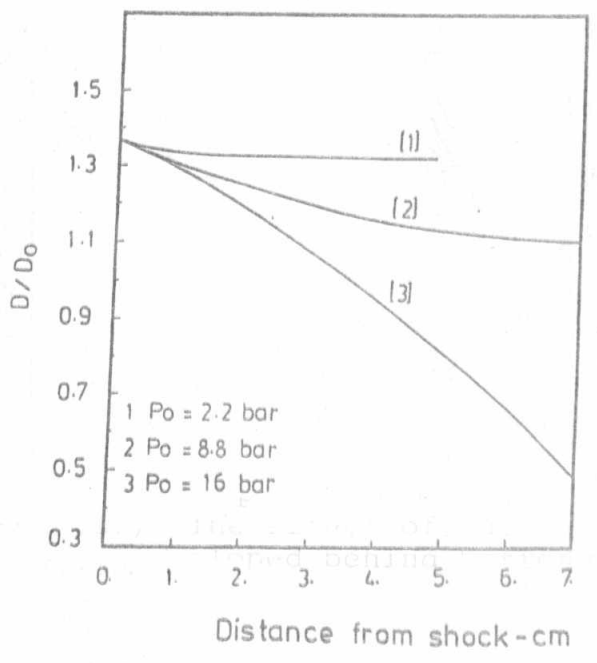


Fig. 6 : Variation of droplet size behind the shock wave (effect of  $P_0$ ).

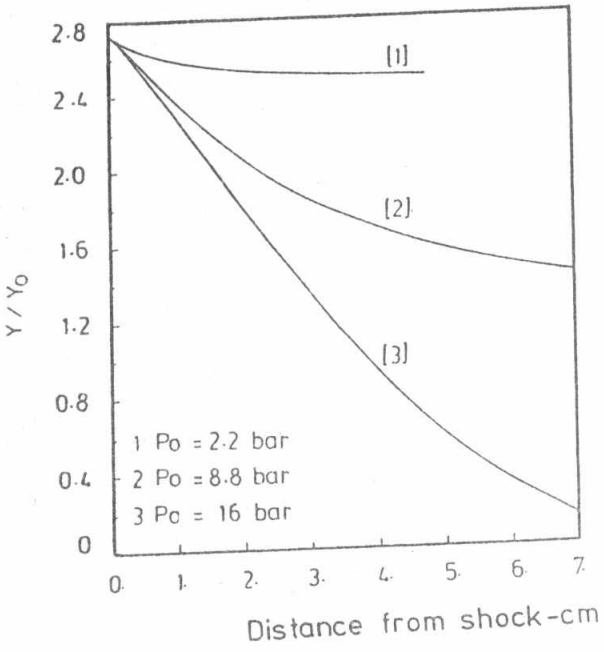


Fig. 7: Variation of steam wetness fraction behind the shock wave (effect of P<sub>0</sub>).

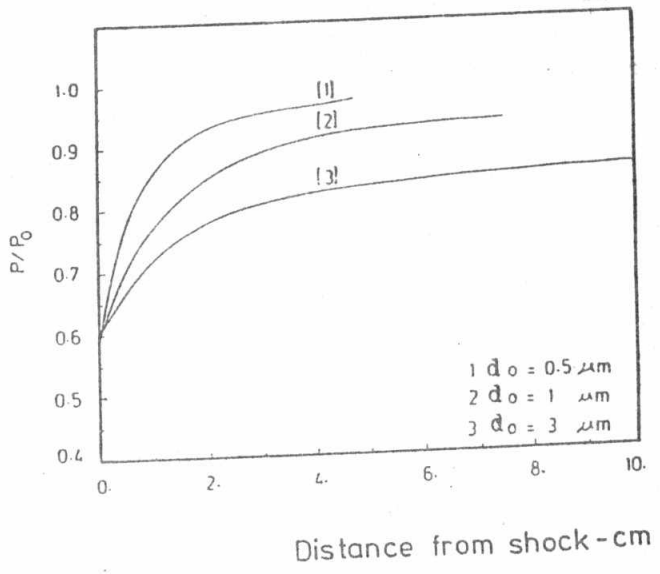


Fig. 8: Variation of flow pressure behind the shock wave (effect of d<sub>0</sub>).

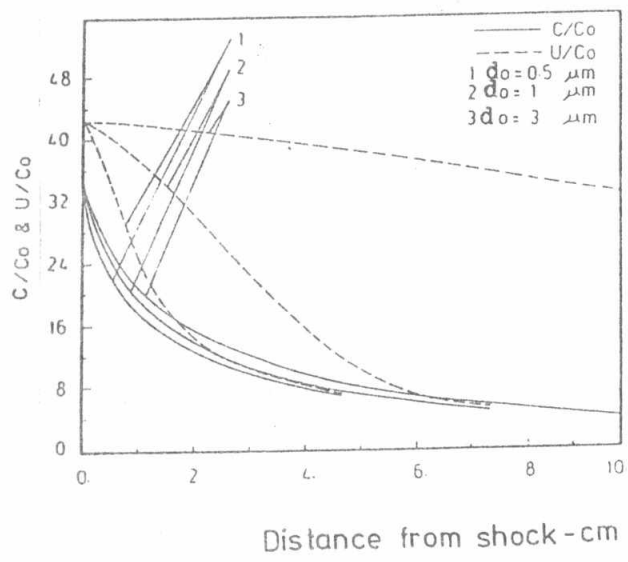


Fig. 9: Variation of vapour and droplet velocities behind the shock wave (effect of d<sub>0</sub>).

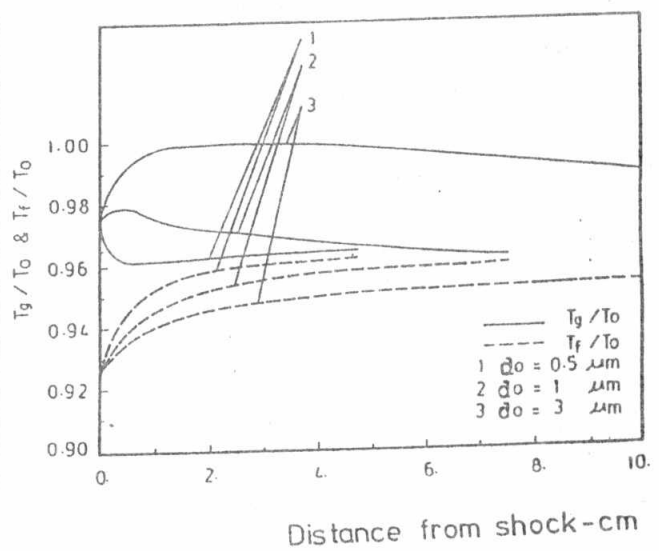


Fig. 10: Variation of vapour and droplet temperatures behind the shock wave (effect of d<sub>0</sub>).

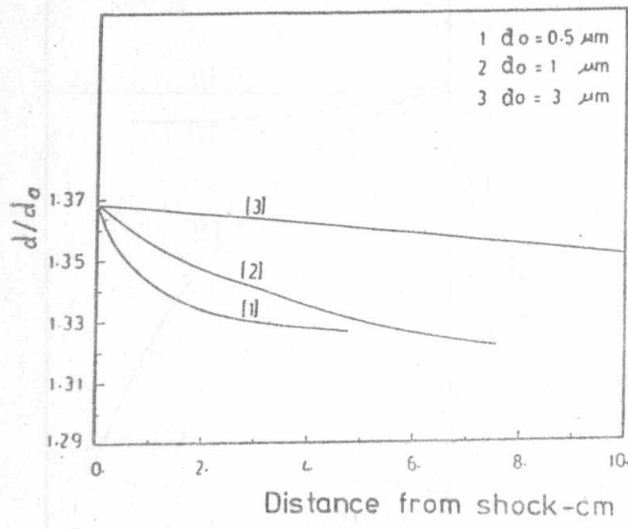


Fig. 11: Variation of droplet size behind the shock wave (effect of  $d_0$ ).

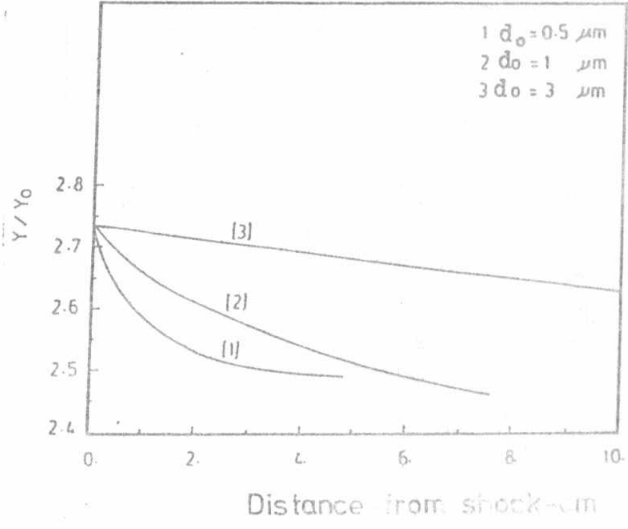


Fig. 12: Variation of steam wetness fraction behind the shock wave (effect of  $d_0$ ).

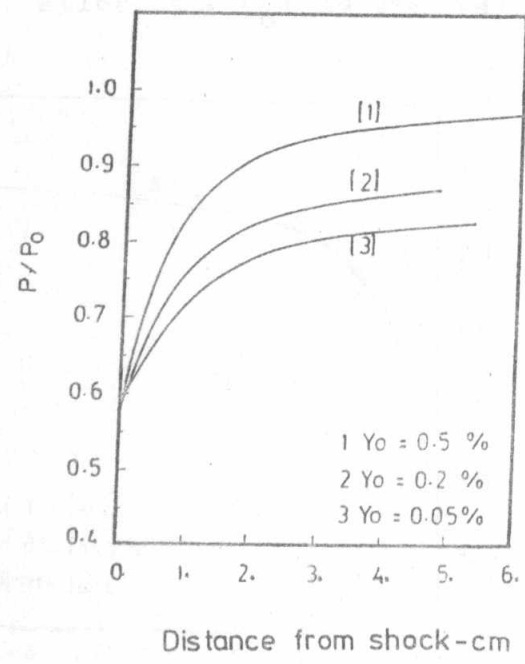


Fig. 13: Variation of flow pressure behind the shock wave (effect of  $Y_0$ ).

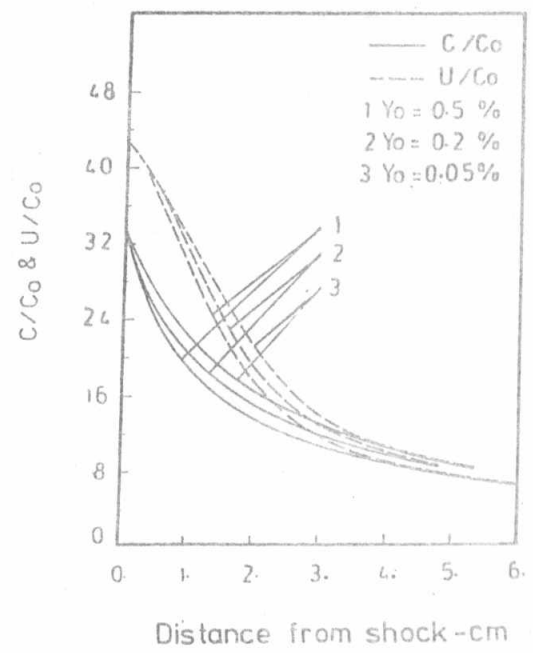


Fig. 14: Variation of vapour and droplet velocities behind the shock wave (effect of  $Y_0$ ).

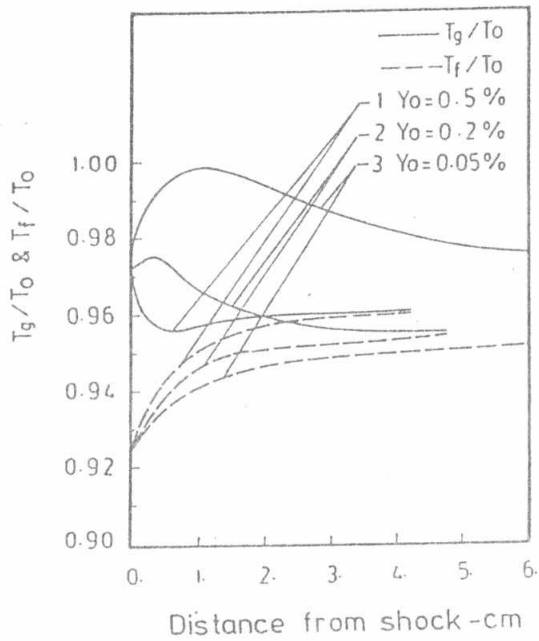


Fig. 15: Variation of vapour and droplet temperatures behind the shock wave (effect of  $Y_o$ ).

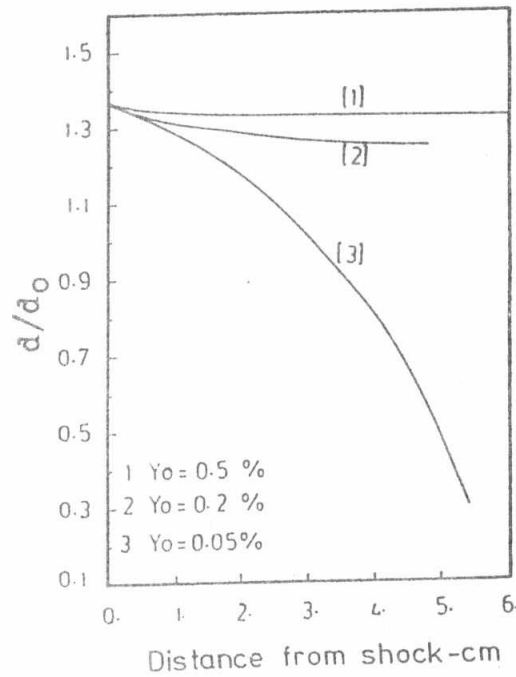


Fig. 16: Variation of droplet size behind the shock wave (effect of  $Y_o$ ).

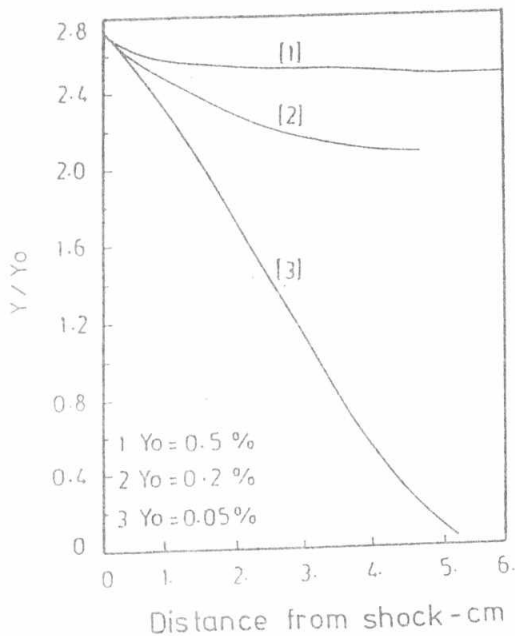


Fig. 17: Variation of steam wetness fraction behind the shock wave (effect of  $Y_o$ ).

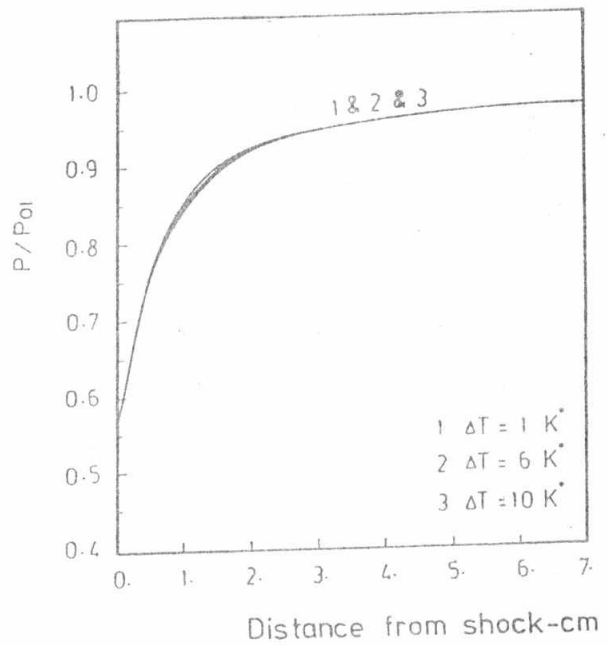


Fig. 18: Variation of flow pressure behind the shock wave (effect of  $\Delta T_o$ ).

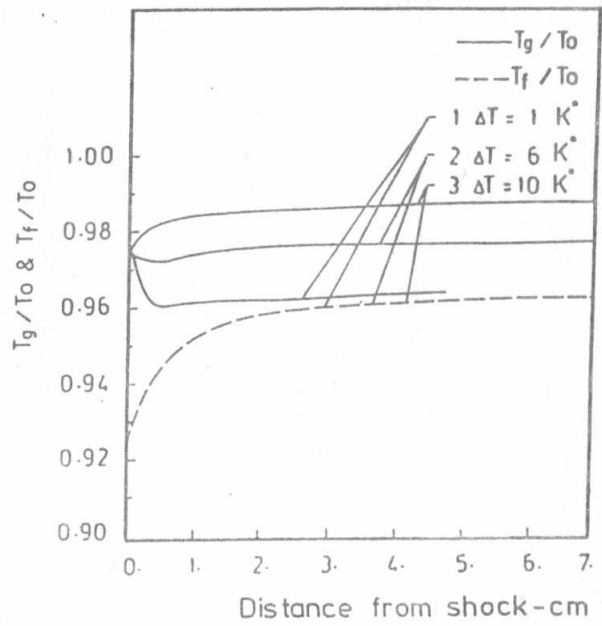
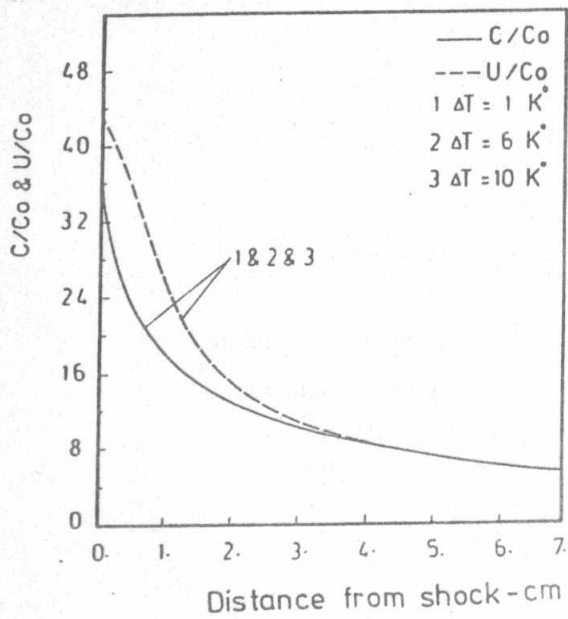


Fig. 19: Variation of vapour and droplet velocities behind the shock wave (effect of  $\Delta T_0$ )

Fig. 20: Variation of vapour and droplet temperatures behind the shock wave (effect of  $\Delta T_0$ )

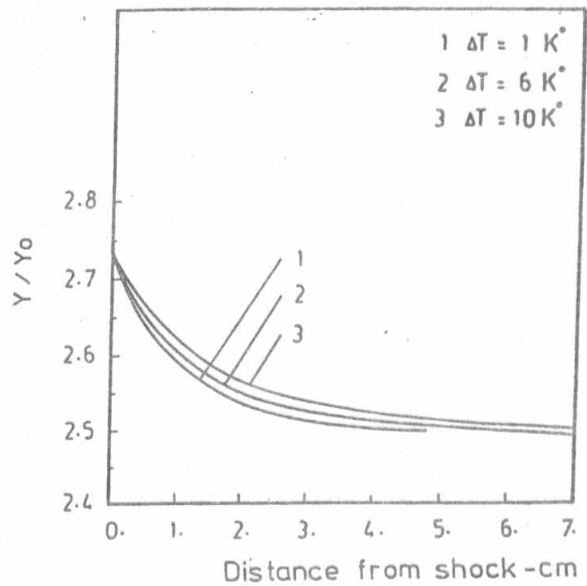
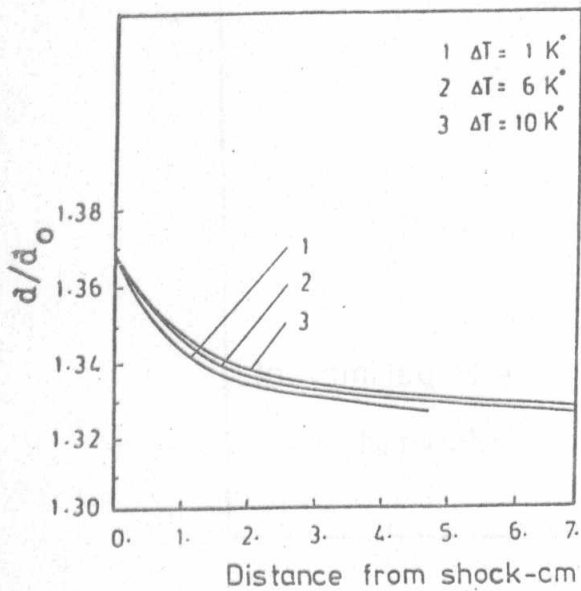


Fig. 21: Variation of droplet size behind the shock wave (effect of  $\Delta T_0$ )

Fig. 22: Variation of steam wetness fraction behind the shock wave (effect of  $\Delta T_0$ )

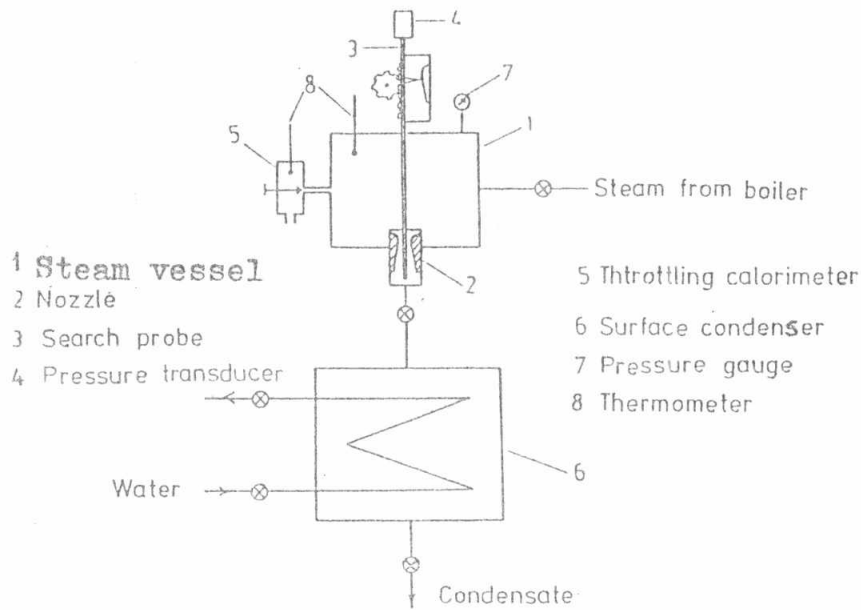


Fig 23: Schematic diagram for the experimental setup.

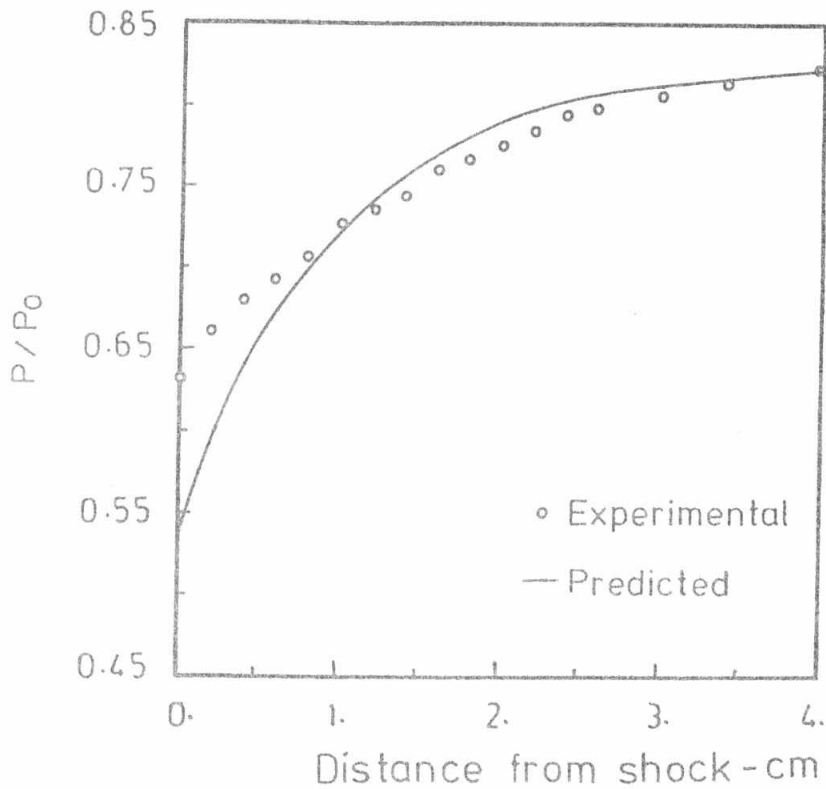


Fig. 24: Plot of experimental values and theoretical predictions for the flow pressure behind the shock wave .